EurJIC European Journal of Inorganic Chemistry

ChemPubSoc Europe

FULL PAPER

DOI:10.1002/ejic.201201118

Selective Synthesis of Vanadium Oxides and Investigation of the Thermochromic Properties of VO_2 by Infrared Spectroscopy

Ming Li,[a] Deng-Bing Li,[a] Jing Pan,[a] Jian-Chao Lin,[a] and Guang-Hai Li*[a]

Keywords: Selective synthesis / Phase transitions / Vanadium / Oxides / Thermochromism / IR spectroscopy

This paper reports a facile and low-cost routine for the selective synthesis of vanadium oxides by hydrothermal treatment of V_2O_5 sol. Our experiments found a defined phase evolution sequence [V_2O_5 → $V_3O_7{\cdot}H_2O$ → VO_2 (B) → VO_2 (A) → VO_2 (M)] that is strongly dependent on the hydrothermal temperature, pressure, and reaction time. A mechanism for the formation of the vanadium oxides based on the oriented attachment (OA) growth model is proposed and discussed. The VO_2 (A + M) phase and the pure VO_2 (M) phase each show an abrupt change in infrared transmittance with temperature, which demonstrates their potential for applications in the field of energy conservation, and the modulation in the infrared properties of the VO_2 (M) phase, thanks to its high purity, is far more prominent than that of the mixture phase VO_2 (A + M).

Introduction

One of the longstanding challenges of crystallization in solid-state chemistry is the capability to predict and to control the occurrence of polymorphism.[1] This matter seems to be far more prominent in the case of vanadium oxides because of the multiple valence states of vanadium. Vanadium oxides have attracted a tremendous attention over recent decades, due to their versatile structures and wide applications in the fields of energy storage and energy conservation.[2]

The phase structures of vanadium oxides have a great influence on their physical and chemical properties. Vanadium dioxide (VO_2) shows an ultrafast first-order reversible metal–semiconductor transition [VO_2 (R)↔VO_2 (M)] at about 68 °C, accompanied by a dramatic change in electrical and optical properties; this reversible structural transition makes VO_2 (M) a very attractive candidate for a variety of technological applications ranging from intelligent thermochromic windows coatings,[3] electrical and infrared light switching devices,[4] and storage media[5] to temperature-sensing devices.[6] Meanwhile, other vanadium oxide phases, such as V_2O_5, V_2O_3, and $V_3O_7{\cdot}H_2O$, are also being extensively explored for applications in the fields of gas sensors,[7] supercapacitor electrodes,[8] and high-energy lithium batteries.[9] In this context, mastery over the phase structures and morphologies of vanadium oxides could optimize their suitabilities for distinctive applications.

Many methods for fabricating vanadium oxide nanostructures have been developed. They include electrospinning,[9b,10] solvothermal[11] and capping-agent-assisted precipitation techniques[12] for V_2O_5, the hydrothermal method for $V_2O_5{\cdot}xH_2O$,[13] $V_2O_4{\cdot}0.25H_2O$,[14] and $V_3O_7{\cdot}H_2O$,[15] vapor-phase transport,[16] pulsed laser deposition,[17] confined-space combustion,[18] and magnetron-sputter[19] for VO_2 (M), and thermal decomposition[20] and plasma hydrogen reduction[21] for V_2O_3. However, a general strategy for producing vanadium oxides with controlled phases and morphologies remains a great challenge, and sometimes special equipment or expensive raw materials are required, which makes the processes far from practical application. Consequently, facile, economical, and selectable syntheses of vanadium oxides are essential for their applications in the energy-saving field.

In this paper we report the synthesis and phase evolution of vanadium oxides by a sol–gel process coupled with a hydrothermal approach. It was found that a definite phase evolution [V_2O_5 → $V_3O_7{\cdot}H_2O$ → VO_2 (B) → VO_2 (A) → VO_2 (M)] takes place with progressive prolongation of hydrothermal time or increasing of reaction temperature, with the morphologies of the vanadium oxides changing from long nanobelt to short nanobelts/nanobeam, and finally to short microrod and snowflake. The formation of vanadium oxides is believed to proceed according to the oriented at-

[a] Key Laboratory of Materials Physics, Anhui Key Laboratory of Nanomaterials and Nanotechnology, Institute of Solid State Physics, Chinese Academy of Sciences,
Hefei 230031, P. R. China
Fax: +86-551-3606266
E-mail: ghli@issp.ac.cn
Homepage: http:/www.issp.ac.cn/

Supporting information for this article is available on the WWW under http://dx.doi.org/10.1002/ejic.201201118.

tachment (OA) model. An abrupt change in the infrared transmittance of the VO_2 (M) phase with temperature was also demonstrated.

Results and Discussion

XRD patterns and SEM (scanning electron microscopy) images of the as-prepared samples obtained at 220 °C after different hydrothermal treatment times are shown in Figures 1 and 2, respectively. One can see that the diffraction peaks of curve (1) in Figure 1 can be indexed to an orthorhombic phase of V_2O_5 (JCPDS card, No. 89-0612) for inorganic V_2O_5 sol without addition of polyethylene glycol (PEG-6000) after hydrothermal treatment for 6 d. The V_2O_5 nanostructures have belt-like shapes with lengths of up to 1 mm, thicknesses less than 40 nm, and widths in the 30–200 nm range (see Figure 2a and b).

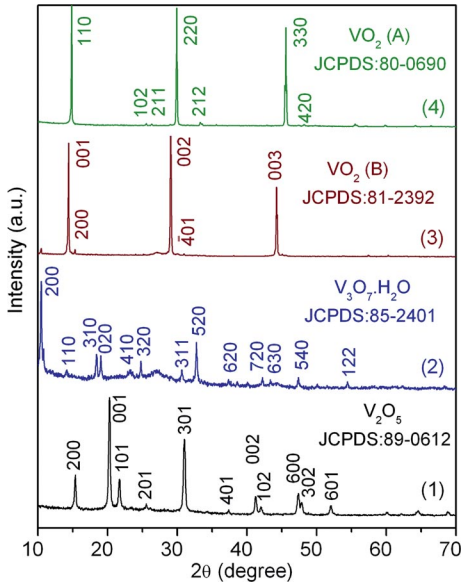

Figure 1. XRD patterns of vanadium oxides hydrothermally treated at 220 °C for (1) 6 d without PEG, and for (2) 1 d, (3) 3 d, and (4) 6 d with PEG.

PEG, as a polymer surfactant, can reduce the valence state of vanadium at a very slow rate.[22] To achieve the synthesis of vanadium oxides with different phase structures, experiments were carried out with progressive increases in hydrothermal times in the presence of PEG. Curve (2) in Figure 1 demonstrates that the $V_3O_7{\cdot}H_2O$ (or $H_2V_3O_8$) phase with an orthorhombic structure (JCPDS 85-2401) was formed after hydrothermal treatment for only 1 d. It is worth noting that there is an amorphous halo at 2θ = 20–30° in curve (2), which is considered to originate from the remnant precursor not having reacted completely after 1 d of hydrothermal treatment, due to the very slow reduction rate of V^{5+} by PEG. The elongated $V_3O_7{\cdot}H_2O$ belt-like structures have diameters of 80–500 nm and thicknesses of 10–60 nm, as shown in Figure 2c and d.

VO_2 (B), one of the metastable phases in the vanadium dioxide family, was formed when the reaction time was prolonged to 3 d. The XRD analysis [curve (3) in Figure 1] showed the monoclinic lattice structure of the obtained VO_2 (B) (JCPDS: 81-2392). In comparison with the ultralong nanobelts of $V_3O_7{\cdot}H_2O$, the rectangle-like VO_2 (B) nanobelts (Figure 2e and f) have become wider (180–560 nm) and thicker (50–100 nm).

When the reaction time was further increased to > 4 d, VO_2 (B) was completely transformed into VO_2 (A) nanobelts [see curve (4) in Figure 1, JCPDS 80-0690]. The widths and thicknesses of the VO_2 (A) nanobelts had increased to 0.5–2.5 μm and 200–450 nm, respectively (see Figure 2g and h).

With further increases either in hydrothermal temperature or in reaction time, a substantial morphologic change takes place. Figures S1a and b in the Supporting Information show two different morphologies of the VO_2 phase after hydrothermal treatment at 240 °C for 10 d: one is microrod, and the other is semi-finished snowflake. Total snowflake VO_2 was formed on hydrothermal treatment at 260 °C for 6 d, as shown in Figure S1c in the Supporting Information. Detailed examination revealed that these snowflakes each consist of six microrods from one center, and have diameters ranging from 0.75 to 3.5 μm, as shown in Figure S1d in the Supporting Information. The layer-by-

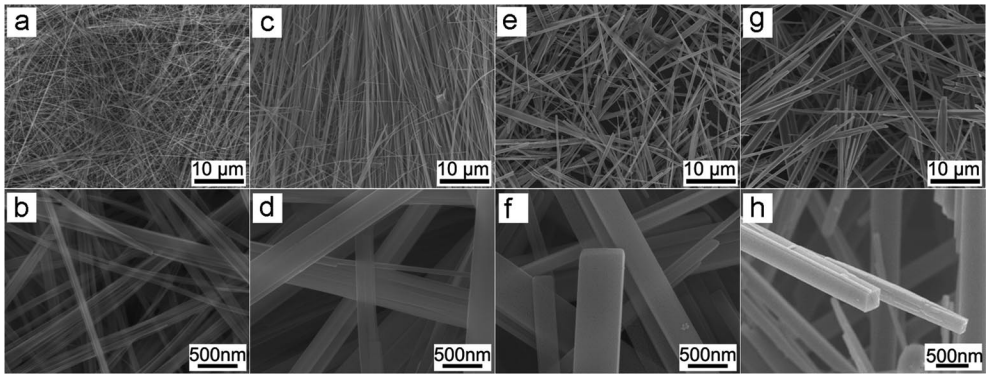

Figure 2. SEM images of the vanadium oxides: (a) and (b) V_2O_5 nanobelts, (c) and (d) $V_3O_7{\cdot}H_2O$ nanobelts, (e) and (f) VO_2 (B) nanobelts, and (g) and (h) VO_2 (A) nanobelts.

layer growth mode can clearly be seen in this figure and is in accordance with the previous report.[23] The corresponding XRD analysis shows that the microrods and snowflakes are a phase mixture of VO_2 (A) and VO_2 (M) [VO_2 (A + M), see Figure S2 in the Supporting Information].

Figure 3 shows the differential scanning calorimetry (DSC) curves of the pure VO_2 (A) phase and the VO_2 (A + M) phase mixture upon warming. An endothermic peak at 161.47 °C can be seen for pure VO_2 (A) phase [curve (1) in Figure 3], corresponding to a reversible phase transition from the low-temperature phase (tetragonal system: $P4_2/ncc$) to the high-temperature phase (body-centered tetragonal system: $I4/m$).[24] For the VO_2 (A + M) phase mixture, the DSC curve shows two endothermic peaks centered at 65.72 °C and 173.43 °C [curve (2) in Figure 3] upon warming; the former can be ascribed to the phase transition of monoclinic VO_2 (M) to rutile VO_2 (R), whereas the latter comes from the phase transition of VO_2 (A). The DSC analyses further confirmed that the phase mixture indeed consists of VO_2 (A) and VO_2 (M).

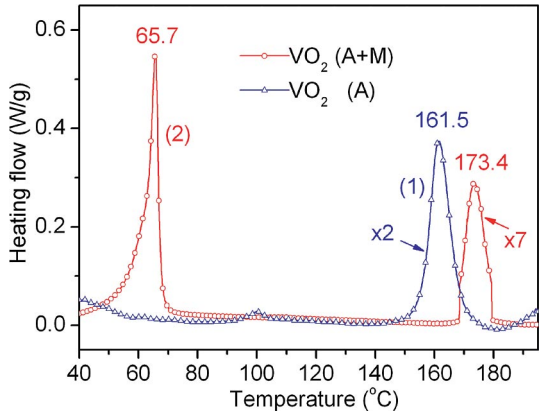

Figure 3. DSC curves of (1) VO_2 (A) phase, and (2) phase mixture of VO_2 (A + M) upon warming.

From the above results we can conclude that vanadium oxides can be selectively synthesized with controllable phase structures under controlled hydrothermal conditions. There is a definite phase progression [$V_2O_5 \rightarrow V_3O_7{\cdot}H_2O \rightarrow VO_2$ (B) $\rightarrow VO_2$(A) $\rightarrow VO_2$ (M)] with increasing hydrothermal time or temperature. Notably, this kind of progression is accompanied by the co-existence of intermediate phase mixtures both between $V_3O_7{\cdot}H_2O$ and VO_2 (B) and between VO_2 (B) and VO_2 (A) (see detail in Figure S3 in the Supporting Information). The corresponding morphologies show regular changes from long nanobelt to short nanobelt, microrods, and finally to snowflakes, and the average sizes of these nanostructures increase accordingly. In fact, the shapes of vanadium oxides can be controlled by changing the relative ratio between PEG and V_2O_5 sol, as demonstrated in our previous study for the VO_2 (B) phase.[25]

With regard to the growth mechanism, the hydrating–exfoliating–splitting model has commonly been used to elucidate the formation of vanadium oxide nanostructures during hydrothermal synthesis.[13,14] By this model, the dimensions of the final product will clearly be smaller than those of the parent structure.[26] This growth mechanism is less evident in this study, because the diameters of vanadium oxides increase with hydrothermal time or temperature. In the case of V_2O_5, our previous study gave strong evidence that the OA model, first reported by Penn and Banfield,[27] is responsible for the self-assembled growth of ultralong nanobelts of V_2O_5.[28] Upon addition of the reductive organic PEG molecules, $V_3O_7{\cdot}H_2O$ was readily formed as a result of the partial reduction of V^{5+} and the formation of V_3O_8 layers in which one oxygen atom from molecular H_2O is held by van der Waals interactions together with hydrogen bonding.[29] With increasing hydrothermal time, the phase transformation between VO_2 polymorphs was triggered after all of the V^{5+} cations had been reduced to V^{4+}, in which the metastable phase VO_2 (B) was preferentially precipitated by recrystallization of the solid in the suspension during hydrothermal treatment. The VO_2 (B) phase then transformed into the relatively stable metastable phase VO_2 (A) by a simple crystallographic slip,[30] which is kinetically more favored than the formation of the most thermodynamic stable rutile structure VO_2 (R).[23] VO_2 (R) eventually formed with further increases either in reaction temperature or in time [the rutile phase VO_2 (R) forms first and is then transformed into the monoclinic polymorph VO_2 (M) upon cooling]. It was found both in our experiments and in previous reports that the autogenous pressure in the sealed autoclave also affects the progression of the phase transformation of VO_2 polymorphs, and that only the VO_2 (B) phase was formed at a low filling ratio.[31] From these results it can be concluded that the hydrothermal temperature, reaction time, and pressure have a synergistic influence on the phase transitions of vanadium oxides.

In addition, PEG has a chain-like structure and is an important factor in the formation of the elongated belt-like vanadium oxides, and the OA growth mechanism also plays an essential role in controlling the aggregation manner of nanobelts. TEM (Figure 4a) clearly shows the elongated belt-like structures characteristic of the intermediate products. Figure 4b and c shows two parts of a single nanobelt, from which one can see that the top part of the nanobelt is composed of several interconnected nanobelts with much smaller dimensions (Figure 4b), and the assembly of these small nanobelts into a whole one can clearly be seen not far from the top of the nanobelt (Figure 4c). This indicates a crystallographic fusion process – a typical feature of the OA growth mechanism. The clear interface between two small nanobelts shown in the HRTEM image of Figure 4d provides further evidence of the crystallographic fusion process. The fact that the adjacent nanobelts have the same crystallographic orientation is consistent with the OA model. The dehydration and recrystallization of a solid in the suspension is associated with the change in the shapes of the vanadium oxides, as illustrated in Figure 2. Furthermore, if the dissolution of a metastable phase under hydrothermal conditions is considered, at a higher temperature

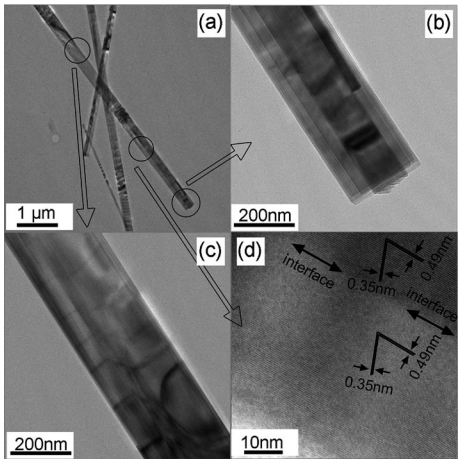

Figure 4. (a), (b), and (c) TEM images of the intermediate vanadium oxide obtained at 220 °C. (d) HRTEM image of the circle part of the nanobelt shown in Figure 4a, demonstrating the interface of two adjacent nanobelts with the same crystallographic orientation.

the rates of nucleation and growth for a thermodynamically stable species on the surface of the preformed structure should be enhanced substantially and thus lead to the decrease in aspect ratio and the formation of multiply-armed microcrystals. The detailed formation process of the vanadium oxides is described in the schematic illustration shown in Figure 5.

The pure VO_2 (M) phase also can be obtained by calcining VO_2 (A) under nitrogen at 600 °C for 1 h, as shown in Figure S4 in the Supporting Information. By comparison with Figure 2g and h, one can see that VO_2 (M) becomes a nanorod with a rounded shape in the lateral direction and has nearly the same length as the VO_2 (A) ultralong nanobelts. The corresponding XRD analysis (Figure 6a) showed that the VO_2 (A) phase had been completely transformed into the VO_2 (M) phase. No other diffraction peaks were detected, indicating that VO_2 (M) is the only phase present. The inset in Figure 6a is the crystal structure of VO_2 (M) viewed along the [001] direction. Figure 6b shows the temperature-dependent resistance of VO_2 (M) pressed from VO_2 (M) powders; an obvious change in the resistivity due to a metal–semiconductor transition can

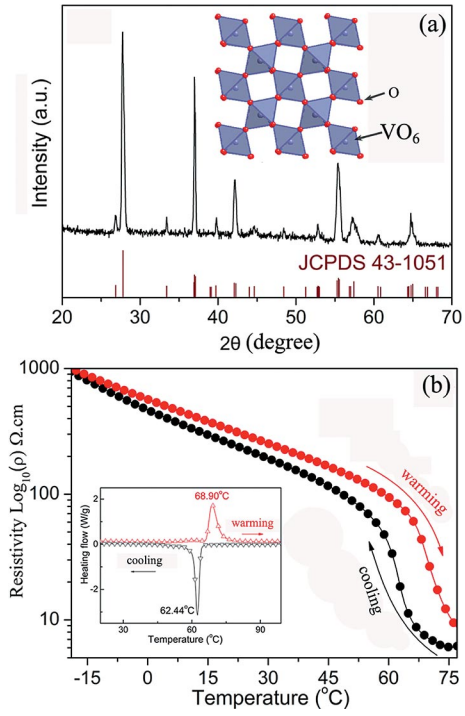

Figure 6. (a) XRD pattern of VO_2 (M) powders; the inset shows the crystal structure viewed along the [001] direction. (b) Temperature dependence of resistivity of VO_2 (M); the inset is the corresponding DSC curve.

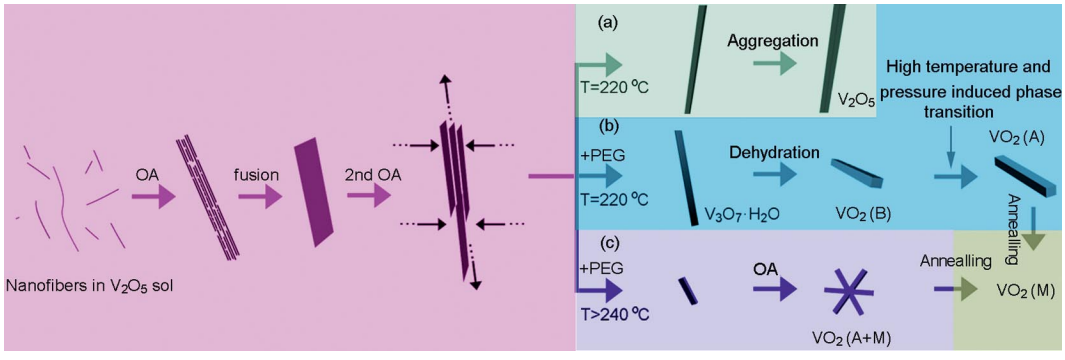

Figure 5. Schematic illustration of the growth of vanadium oxides by the OA mechanism. At the early stage of the hydrothermal reaction, the V_2O_5 nanofibers in the sol are oriented suitably to become attached to one another, and the subsequent coalescence and oriented assembly then leads to the formation of the thin, belt-like structure. Without the addition of PEG: (a) the final product is V_2O_5 ultralong nanobelts. With the addition of PEG: (b) at 220 °C, firstly $V_3O_7{\cdot}H_2O$ forms, due to partial reduction of V^{5+} to V^{4+}. Then, as a result of valence reduction and dehydration processes, VO_2 (B) forms. Finally, the phase transformation from VO_2 (B) to VO_2 (A) takes place easily under hydrothermal conditions with relatively high temperatures and pressures. (c) At 240 °C, the dissolution of the metastable phase leads to a decrease in aspect ratio and the formation of multiple-armed microcrystals (the increased sizes should reduce the dissolution rate). Meanwhile, the thermodynamically most stable phase – VO_2 (M) – forms together with VO_2 (A). Subsequently, high-purity VO_2 (M) is obtained by annealing treatment.

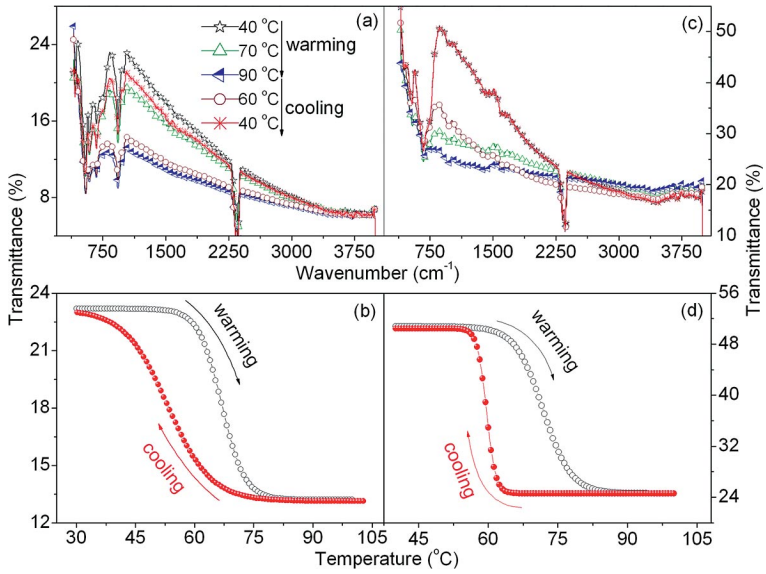

Figure 7. Variable-temperature infrared spectra: (a) and (b) of the VO_2 (A + M) phase mixture, and (c) and (d) of the VO_2 (M) phase.

clearly be seen at about 68 °C. The corresponding DSC analysis (inset in Figure 6b) shows that the endothermic and exothermic peaks are sharp and symmetrical, indicting a reversible phase transition feature of the VO_2 (M).

Figure 7 shows variable-temperature infrared transmittance spectra of the VO_2 (A + M) phase mixture and the VO_2 (M) pure phase over a thermal cycle, which gives strong evidence that both of them are potential candidates for application in the field of energy conservation through light control. The infrared transmittance of VO_2 (A + M) gradually decreases with increasing temperature (from 30 to 60 °C in the heating process), then drops quickly from 60 to 75 °C, and finally falls to a nearly constant value [see Figure 7a and b (infrared transmittance at 1030 cm^{-1})]. The opposite infrared transmittance changes were also observed in the cooling process. A similar change in IR transmittance can be observed for the pure VO_2 (M) phase, as shown in Figure 7c and d, and the corresponding transition temperatures are in accordance with the DSC result shown in Figure 6b. The modulation in the infrared properties of the pure VO_2 (M) phase, thanks to its high purity, is far more prominent than in the case of the VO_2 (A + M) phase mixture.

Conclusions

A facile and low-cost strategy for the selective synthesis of vanadium oxides by hydrothermal treatment of inorganic V_2O_5 sol, either in the presence or in the absence of PEG, has been proposed. A specific phase evolution process [$V_2O_5 \rightarrow V_3O_7{\cdot}H_2O \rightarrow VO_2$ (B) $\rightarrow VO_2$ (A) $\rightarrow VO_2$ (M)] under the synergistic influence of hydrothermal temperature, pressure, and reaction time was found. The morphologies of the vanadium oxides change from long nanobelts to nanobelts/nanorods, and finally to short microrods and snowflakes in a manner consistent with the oriented attachment growth model. Variable-temperature mid-infrared transmittance analyses demonstrate potential applications of VO_2 (M) in the field of energy conservation. Our method might be extendable to the preparation of other materials through the self-assembly of nanoscale building blocks by hydrothermal treatment.

Experimental Section

Preparation of Vanadium Oxides: V_2O_5 sol was obtained through a melt quenching process. V_2O_5 powder (99.9%) was heated to 850 °C in a crucible until molten and was then quickly poured into distilled water at room temperature. After vigorous stirring for 1 d, a red V_2O_5 sol was obtained. In a typical reaction, a certain amount of polyethylene glycol (PEG-6000, 0.3–2 g) was added to the inorganic V_2O_5 sol (40 mL) to form a homogeneous precursor after stirring for a few hours. The precursor was placed in a 50 mL Teflon cup that was then heated at temperatures between 220 °C and 260 °C for different times in a sealed autoclave with a stainless steel shell. The precipitate obtained upon cooling to room temperature was washed several times with deionized water and ethanol and then dried at 70 °C in air.

Sample Characterization: The morphologies of the as-prepared samples were examined by SEM (Sirion 200) and TEM (JEM-2010). The phase structures were investigated by XRD with use of the Cu-$K_{\alpha 1}$ line (Philips X'Pert).

Determination of Properties: DSC analysis was performed with a Dupont differential thermal analyzer under a flow of nitrogen with a heating rate of 10 °C min^{-1}. FTIR spectroscopy was performed with a Bruker Vector-22 FTIR spectrometer. A physical properties measurement system (PPMS) was used to evaluate the temperature dependence of the resistance properties of the pressed powders with dimensions of 5 × 2 × 2 mm in a four-probe model.

Supporting Information (see footnote on the first page of this article): SEM images of VO_2 on hydrothermal treatment at 240 °C for 10 d and at 260 °C for 6 d (Figure S1); XRD pattern of the VO_2 (A + M) phase mixture obtained under the hydrothermal con-

ditions of curve (1) (240 °C, 10 d) and curve (2) (260 °C, 6 d) (Figure S2); XRD patterns of vanadium oxide intermediates of $V_3O_7{\cdot}H_2O$ and VO_2 (B), and VO_2 (B) and VO_2 (A) (Figure S3); SEM images of VO_2 (M) obtained by annealing VO_2 (A) at 600 °C (Figure S4).

Acknowledgments

This work was financially supported by the National Basic Research Program of China (2009CB939903), and the innovation project of the Chinese Academy of Sciences (KJCX2-YW-H2O).

[1] A. W. Xu, W. F. Dong, M. Antonietti, H. Cölfen, *Adv. Funct. Mater.* **2008**, *18*, 1307–1313.
[2] a) P. Y. Zavalij, M. S. Whittingham, *Acta Crystallogr., Sect. B* **1999**, *55*, 627–663; b) C. Wu, Y. Xie, *Energy Environ. Sci.* **2010**, *3*, 1191–1206.
[3] I. P. Parkin, T. D. Manning, *J. Chem. Educ.* **2006**, *83*, 393.
[4] M. Rini, Z. Hao, R. W. Schoenlein, C. Giannetti, F. Parmigiani, S. Fourmaux, J. C. Kieffer, A. Fujimori, M. Onoda, S. Wall, A. Cavalleri, *Appl. Phys. Lett.* **2008**, *92*, 181904.
[5] I. Balberg, S. Trokman, *J. Appl. Phys.* **1975**, *46*, 2111–2119.
[6] B. J. Kim, Y. W. Lee, B. G. Chae, S. J. Yun, S. Y. Oh, H. T. Kim, Y. S. Lim, *Appl. Phys. Lett.* **2007**, *90*, 023515.
[7] a) X. W. J. Liu, Q. Peng, Y. Li, *Adv. Mater.* **2005**, *17*, 764–767; b) A. V. Grigorieva, S. M. Badalyan, E. A. Goodilin, M. N. Rumyantseva, A. M. Gaskov, A. Birkner, Y. D. Tretyakov, *Eur. J. Inorg. Chem.* **2010**, 5247–5253.
[8] a) G. Wee, H. Z. Soh, Y. L. Cheah, S. G. Mhaisalkar, M. Srinivasan, *J. Mater. Chem.* **2010**, *20*, 6720–6725; b) H. Liu, P. He, Z. Li, D. Sun, H. Huang, J. Li, G. Zhu, *Chem. Asian J.* **2006**, *1*, 701–706.
[9] a) J. Yan, A. Sumboja, E. Khoo, P. S. Lee, *Adv. Mater.* **2011**, *23*, 746–750; b) D. Yu, C. Chen, S. Xie, Y. Liu, K. Park, X. Zhou, Q. Zhang, J. Li, G. Cao, *Energy Environ. Sci.* **2011**, *4*, 858–861; c) S. Wang, S. Li, Y. Sun, X. Feng, C. Chen, *Energy Environ. Sci.* **2011**, *4*, 2854–2857; d) Y. Zhang, M. Fan, X. Liu, C. Huang, H. Li, *Eur. J. Inorg. Chem.* **2012**, 1650–1659.
[10] H. G. Wang, D. L. Ma, Y. Huang, X. B. Zhang, *Chem. Eur. J.* **2012**, *18*, 8987–8993.
[11] S. A. Corr, M. Grossman, Y. F. Shi, K. R. Heier, G. D. Stucky, R. Seshadri, *J. Mater. Chem.* **2009**, *19*, 4362–4367.
[12] B. Saravanakumar, K. K. Purushothaman, G. Muralidharan, *ACS Appl. Mater. Interfaces* **2012**, *4*, 4484–4490.
[13] B. Li, Y. Xu, G. Rong, M. Jing, Y. Xie, *Nanotechnology* **2006**, *17*, 2560.
[14] M. Wei, H. Sugihara, I. Honma, M. Ichihara, H. Zhou, *Adv. Mater.* **2005**, *17*, 2964–2969.
[15] G. C. Li, S. P. Pang, Z. B. Wang, H. R. Peng, Z. K. Zhang, *Eur. J. Inorg. Chem.* **2005**, 2060–2063.
[16] a) J. I. Sohn, H. J. Joo, A. E. Porter, C. J. Choi, K. Kim, D. J. Kang, M. E. Welland, *Nano Lett.* **2007**, *7*, 1570–1574; b) C. Piccirillo, R. Binions, I. P. Parkin, *Eur. J. Inorg. Chem.* **2007**, 4050–4055; c) Y. Cheng, T. Zhang, Y. Cai, K. M. Ho, K. K. Fung, N. Wang, *Eur. J. Inorg. Chem.* **2010**, 4332–4338.
[17] J. Y. Suh, R. Lopez, L. C. Feldman, J. R. F. Haglund, *J. Appl. Phys.* **2004**, *96*, 1209–1213.
[18] C. Wu, J. Dai, X. Zhang, J. Yang, F. Qi, C. Gao, Y. Xie, *Angew. Chem.* **2010**, *122*, 138; *Angew. Chem. Int. Ed.* **2010**, *49*, 134–137.
[19] D. Brassard, S. Fourmaux, M. Jean-Jacques, J. C. Kieffer, M. A. E. Khakani, *Appl. Phys. Lett.* **2005**, *87*, 051910.
[20] Y. Ishiwata, T. Shiraishi, N. Ito, S. Suehiro, T. Kida, H. Ishii, Y. Tezuka, Y. Inagaki, T. Kawae, H. Oosato, E. Watanabe, D. Tsuya, M. Nantoh, K. Ishibashi, *Appl. Phys. Lett.* **2012**, *100*, 043103.
[21] F. Y. Kong, M. Li, D. B. Li, Y. Xu, Y. X. Zhang, G. H. Li, *J. Cryst. Growth* **2012**, *346*, 22–26.
[22] L. Kong, Z. Liu, M. Shao, Q. Xie, W. Yu, Y. Qian, *J. Solid State Chem.* **2004**, *177*, 690–695.
[23] C. Cao, Y. Gao, H. Luo, *J. Phys. Chem. C* **2008**, *112*, 18810–18814.
[24] a) Y. Oka, S. Sato, T. Yao, N. Yamamoto, *J. Solid State Chem.* **1998**, *141*, 594–598; b) S. Zhang, B. Shang, J. Yang, W. Yan, S. Wei, Y. Xie, *Phys. Chem. Chem. Phys.* **2011**, *13*, 15873–15881.
[25] M. Li, F. Y. Kong, Y. X. Zhang, G. H. Li, *CrystEngComm* **2011**, *13*, 2204–2207.
[26] G. Li, S. Pang, L. Jiang, Z. Guo, Z. Zhang, *J. Phys. Chem. B* **2006**, *110*, 9383–9386.
[27] J. F. Banfield, S. A. Welch, H. Zhang, T. T. Ebert, R. L. Penn, *Science* **2000**, *289*, 751–754.
[28] M. Li, F. Kong, H. Wang, G. Li, *CrystEngComm* **2011**, *13*, 5317–5320.
[29] H. Li, T. Zhai, P. He, Y. Wang, E. Hosono, H. Zhou, *J. Mater. Chem.* **2011**, *21*, 1780–1787.
[30] J. Galy, *J. Solid State Chem.* **1999**, *148*, 224–228.
[31] a) S. Ji, F. Zhang, P. Jin, *J. Solid State Chem.* **2011**, *184*, 2285–2292; b) S. D. Ji, Y. G. Zhao, F. Zhang, P. Jin, *J. Ceram. Soc. Jpn.* **2010**, *118*, 867–871.

Received: September 21, 2012
Published Online: December 17, 2012

